

Copyright WILEY-VCH Verlag GmbH & Co. KGaA, 69469 Weinheim, Germany,

2018.

Supporting Information

Activating Inert Sites in Cobalt Silicate Hydroxides for Oxygen Evolution through Atomically Doping

*Jiexin Zhu, Lixue Xia, Wenxuan Yang, Ruohan Yu, Wei Zhang, Wen Luo, Yuhang Dai, Wei Wei, Liang Zhou, Yan Zhao, * Liqiang Mai**

Experimental section

Chemicals. Sodium metasilicate nonahydrate ($\text{Na}_2\text{SiO}_3 \cdot 9\text{H}_2\text{O}$, 98%), cobalt chloride hexahydrate ($\text{CoCl}_2 \cdot 6\text{H}_2\text{O}$, Analytical Reagent), iron sulfate heptahydrate ($\text{FeSO}_4 \cdot 7\text{H}_2\text{O}$, Analytical Reagent), and potassium hydroxide (KOH, 99.999%) were purchased from Aladdin Industrial Inc. (Shanghai, China). All the chemicals were used without further purification.

Synthesis of CSHNs and FCHNs electrocatalysts. The CSHNs were prepared by a hydrothermal method. In a typical procedure, $\text{Na}_2\text{SiO}_3 \cdot 9\text{H}_2\text{O}$ (2.0 mmol) and $\text{CoCl}_2 \cdot 6\text{H}_2\text{O}$ (3.0 mmol) were dissolved in 40 mL of deionized water, respectively, and stirred vigorously for 15 min. Then, two solutions were mixed and stirred for another 10 min. Afterward, the solution described above was transferred into a sealed Teflon-lined stainless steel autoclave and subsequently annealed at 200 °C for 24 h. The obtained cobalt phyllosilicate powder was washed several times with deionized water before drying by vacuum freeze-drying. The preparation process of FCSHNs-3, FCSHNs-6, and FCSHNs-10 was similar to that of CSHNs, except that 3%, 6% and 10% of $\text{CoCl}_2 \cdot 6\text{H}_2\text{O}$ was replaced by equimolar $\text{FeSO}_4 \cdot 7\text{H}_2\text{O}$ and keep the total number of moles at 3.0 mmol.

Materials characterizations. The as-synthesized products were characterized with a D8 Advance X-ray diffractometer using $\text{Cu-K}\alpha$ radiation ($\lambda = 1.5418 \text{ \AA}$). Transmission electron microscope (TEM) images, high angle annular dark field imaging-scanning TEM (HAADF-STEM), energy dispersive spectroscopy elemental mappings, and electron energy-loss spectroscopy (EELS) spectra were obtained using a double spherical aberration corrected transmission electron microscope (Titan Cubed Themis G2 300/Titan Cubed Themis G2 30). Fourier transform infrared (FTIR) transmittance spectra were recorded using a Nicolet 6700 (Thermo Fisher Scientific Co., USA) IR spectrometer. X-ray photoelectron spectroscopy (XPS) measurements were performed using a VG MultiLab 2000 instrument. Temperature-dependent magnetic susceptibility plots were measured in the temperature range from 50 to 300 K under $H = 2 \text{ kOe}$ with

a Magnetic Property Measurement System model SQUID-VSM (Quantum Design, USA). Thickness characterization is performed by atomic force microscope (AIST, AIST-NT SmartSPM).

Electrochemical tests. The CSHNs and FCSHNs powder electrocatalyst inks were prepared using a mixture of 0.1 mL deionized water, 0.85 mL ethanol, 0.05 mL 5 wt% Nafion solution, 5 mg of the catalysts and 5 mg carbon black (Vulcan XC-72R) followed by ultrasonication for 1 h. Then, 10 μL of the ink was uniformly loaded onto a freshly polished glassy-carbon electrode (GCE, diameter = 0.5 cm), which was used as the working electrode yielding a catalyst loading of 0.25 mg cm^{-2} .

All the OER electrochemical measurements of the prepared electrodes were performed by a conventional three-electrode system using an electrochemical workstation (CHI 760D, Shanghai Chenhua Instrument Co. Ltd.) and modulated speed rotator (MSR, AFMSRCE, rotate speed: 50-10000 rpm, PINE) in a 1.0 M KOH (pH = 13.7) aqueous solution. The GCE with electrocatalysts ink was used as the working electrode, while platinum plate (Pt, 1 cm \times 1 cm) and Hg/HgO (0.098 V versus a standard hydrogen electrode filled with 1.0 M NaOH solution) were used as the counter electrode, and reference electrode. The rotate speed of MSR was keep at 1600 rpm. The potential values were referenced to the reversible hydrogen electrode (RHE) according to the formula $E(\text{RHE}) = E(\text{Hg/HgO}) + 0.098 + 0.059 \times \text{pH}$. Prior to recording the electroactivity of the catalysts, the electrochemical accessibility of the working electrode was optimized by potential cycling between 1.1 and 1.7 V at 100 mV s^{-1} in 1.0 M KOH until stable voltammogram curves were obtained. Then, the polarization curves were recorded at a scan rate of 1 mV s^{-1} and the overpotential (η) at $j = 10 \text{ mA cm}^{-2}$ was determined using the following equation: $\eta = E \text{ (vs. RHE)} - 1.23 \text{ V}$. Tafel plots of the samples were obtained by plotting potential against the logarithm of j using the Tafel equation ($\eta = a \log j + b$, where a is the slope and b is a constant). A long-term stability test was performed at $j = 10 \text{ mA cm}^{-2}$ for 24 h. The double layer capacitance of electrocatalysts was estimated by performing CV at different scan rates of 10, 20, 30, 40, 50, 60, 70, 80, 90 and 100 mV s^{-1} , followed by extracting the slope from the

resulting $|j_a - j_c|/2$ vs. ν plots (j_a and j_c represent the anodic and cathodic current densities at the middle of the applied potential). The electrochemical impedance spectroscopy (EIS) was carried out in a frequency range from 100 kHz to 10 MHz at the overpotential of 300 mV. All the electrochemical measurements were conducted at room temperature. TOF values were calculated according to the following equation: $\text{TOF} = j \times A / (4 \times F \times n)$, where j is the current density at a given potential, A is the surface of the electrode, n is the mole number of metal atoms on the electrode, and F is Faraday constant. Note that, in the calculations all metal atoms are assumed to be catalytically active. However, because a fraction of metal sites might not contribute to the catalytic reaction, the calculated TOF represents a lower limit.

X-ray absorption measurements. The Co and Fe K -edge X-ray absorption near-edge spectroscopy (XANES) and extended X-ray absorption fine structure (EXAFS) spectra were collected at room temperature in transmission mode at beamline 1W1B of the Beijing Synchrotron Radiation Facility (BSRF), using a Si (111) double-crystal monochromator. The storage ring of BSRF was operated at 2.5 GeV with a maximum current of 250 mA in decay mode. The energy was calibrated using Co/Fe foil, and the intensity of the incident and transmitted X-rays was monitored by standard N₂-filled ion chambers. The powdered samples were uniformly mixed with BN powder and pressed to a pellet to achieve the best signal-to-noise ratio. A detuning of about 20% by misaligning the silicon crystals was also performed to suppress the high harmonic content. The Co and Fe K -edge XANES and EXAFS spectra were also performed on beamline BL14W1 at Shanghai Synchrotron Radiation Facility (SSRF) with a ring electron current of 250 mA at 3.5 GeV and appropriate absorption edge jump were measured in transmission mode

XANES spectra of the Co and Fe L -edge were measured at the beamline U19 of National Synchrotron Radiation Laboratory (NSRL) in Hefei under a total electron yield (TEY) mode by collecting the sample drain current.

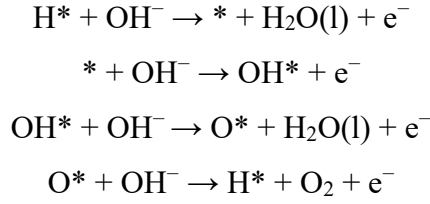
The X-ray absorption fine structure (XAFS) raw data were background-subtracted, normalized, and Fourier transformed by standard procedures with the ATHENA

program.

In-situ Raman measurements. Raman spectra was obtained by Horiba LabRAM HR Evolution. The Raman spectra were acquired with He/Ne laser of $\lambda = 532$ nm and 4.9 mW. The cyclic voltammetry (CV) curves were performed by an electrochemical workstation (Autolab PGSTAT 204) in a customized Teflon cell with 0.1 M KOH solution. A gold disk electrode worked as the working electrode, an Hg/HgO electrode as the reference electrode and a polished platinum wire as the counter electrode. The prepare process of electrocatalysts ink is the same as the process described aboved. Then, 5 μ L of the ink was uniformly loaded onto a freshly polished gold disk electrode (diameter = 0.3 cm), which was used as the working electrode. The potential values were referenced to the RHE without iR corrected. To exclude the disturb of produced bubbles, each curve is recorded after adjusting the focal length.

Calculation Methods and Models. All density functional theory (DFT) calculations on various concentration of Fe doped cobalt phyllosilicate nanosheets (FCSHNs) with layered crystalline motifs system, including density of states (DOS), band structure and electron density difference, have been conducted by Vienna *ab initio* simulation package (VASP)^[1-2] using the PBE functional^[3-4] and the projector augmented wave (PAW)^[5-6] method. Structural optimization and DOS calculations were conducted on the same plane-wave cutoff energy, 450 eV, and the same $3 \times 2 \times 2$ Monkhorst-Pack mesh^[7] for the integration of Brillouin zone, and $1 \times 1 \times 1$ Monkhorst-Pack mesh was used to calculate the adsorption energy for the sake of computational cost. The optimized geometries converged until the force acting on each atom being less than 0.05 eV/Å and the energy converging within 10^{-5} eV. Gaussian smearing scheme^[8] with a smearing parameter of 0.2 eV was applied in the optimization calculations, while tetrahedron method with Blöchl corrections adopted in the DOS calculations.

Four-step reaction mechanism proposed by Goodenough et al.^[9] for the OER reaction has been adopted in the calculations aiming for detecting the difference of catalytic activity among metal silicate hydroxides. The crystal structure is similar to the reported ones by Ju Seong Kim et al.^[10] The four-electron reaction steps were listed as follows:



(* denotes the structure with one bald oxygen surface site and X* representing the structures adsorbing X species)

The Gibbs free energy differences for the four reaction steps were calculated using the following steps:

$$\begin{aligned}
\Delta G_1 &= G(*) + G(\text{H}_2\text{O}) - G(\text{H}^*) - G(\text{OH}^- - \text{e}^-) - eU \\
\Delta G_2 &= G(\text{OH}^*) - G(*) - G(\text{OH}^- - \text{e}^-) - eU \\
\Delta G_3 &= G(\text{O}^*) + G(\text{H}_2\text{O}) - G(\text{OH}^*) - G(\text{OH}^- - \text{e}^-) - eU \\
\Delta G_4 &= G(\text{H}^*) + G(\text{O}_2) - G(\text{O}^*) - G(\text{OH}^- - \text{e}^-) - eU \\
G &= \text{ZPE} - \text{TS} + E_v
\end{aligned}$$

The electronic energies of surface adsorption complexes and gases were obtained from the density functional theory calculations. The entropy S and the internal thermal energy E_v were calculated by the following equations, only the contribution from vibration considered for the surface adsorption complex.

$$\begin{aligned}
S &= R \left\{ \frac{\theta_v/T}{e^{\theta_v/T} - 1} - \ln(1 - e^{-\theta_v/T}) \right\} \\
E_v &= R \sum_v \theta_v \left(\frac{1}{2} + \frac{1}{e^{\theta_v/T} - 1} \right)
\end{aligned}$$

where θ_v is the vibrational temperature being equal to hcv/k , ν is the vibrational wavenumber, and T is set to 298 K. The ZPE-TS values of H_2O , H_2 are equal to -0.11 and -0.14 eV, respectively, of which the vibrational frequencies and the entropy were taken at room temperature and 1 bar pressure (not including H_2O) from the NIST-JANAF thermodynamics table^[11]. The entropy of water was taken at 0.035 bar which is the equilibrium pressure between gas-phase water and liquid water at room temperature. The free energy of O_2 was calculated from the reaction $\text{H}_2\text{O} \rightarrow \frac{1}{2} \text{O}_2 + \text{H}_2$, of which the experimental free energy change is 2.46 eV, because the electronic structure of O_2 was difficult to define accurately with DFT. Within the SHE method^[12], the effect of the existing one electron in the electrode was considered by the addition of $-eU$, where U equals the experimental electrode potential relative to the standard hydrogen electrode, 1.6 V. The Gibbs free energy of $\text{OH}^- - \text{e}^-$ was calculated by the following equation,

$$G(\text{OH}^- - e^-) = G(\text{H}_2\text{O}) - \frac{1}{2} G(\text{H}_2) + k_B T \ln(10 \cdot \text{pH})$$

where the last term is the correction to the free energy of OH^- anions at a $\text{pH} \neq 0$ (here, $\text{pH} = 13$), k_B is the Boltzmann constant. The theoretical overpotential could be expressed as the difference of the maximum of ΔG and the average value among the four OER steps, $\eta_{\text{OER}} = \Delta G_{\text{max}}/e - 0.37 \text{ V}$.

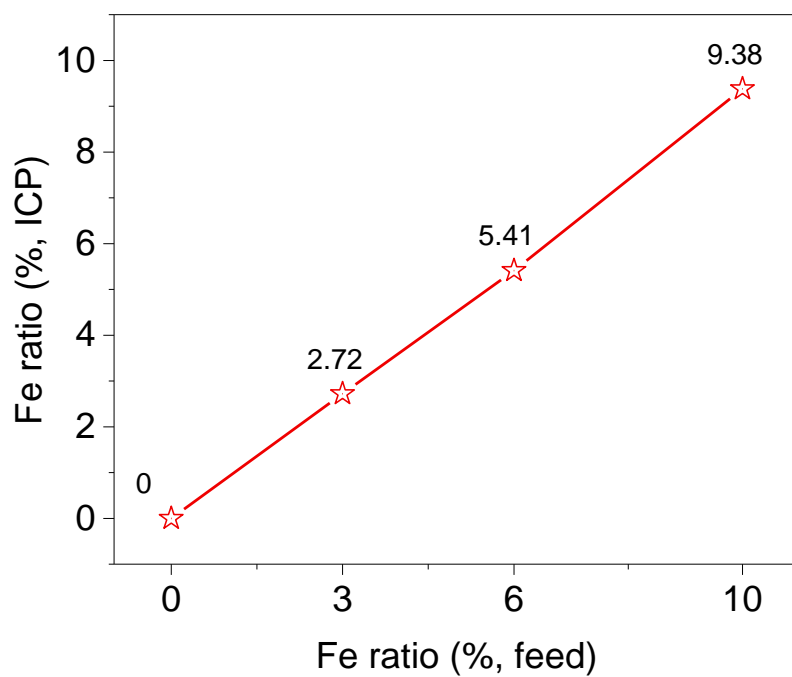


Figure S1. Fe/Co ratios of the samples determined by ICP.

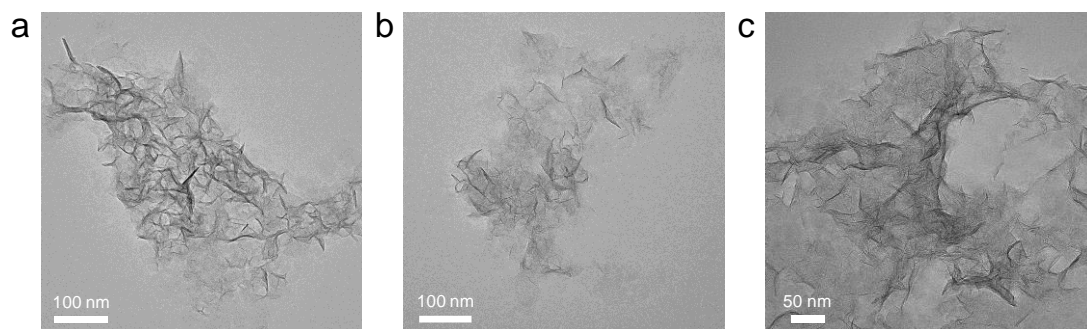


Figure S2. TEM images of (a) CSHNs, (b) FCSHNs-3, and (c) FCSHNs-10.

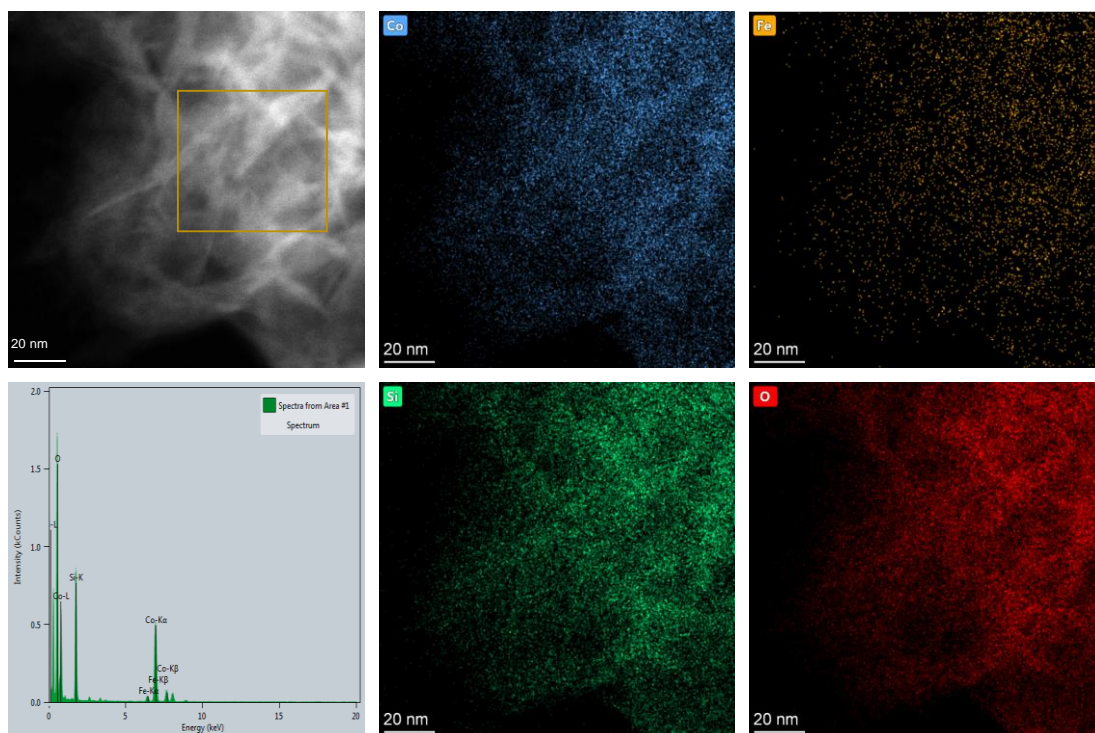


Figure S3. HAADF-STEM image, EDX spectrum, and EDX elemental mappings of FCSHNs-6.

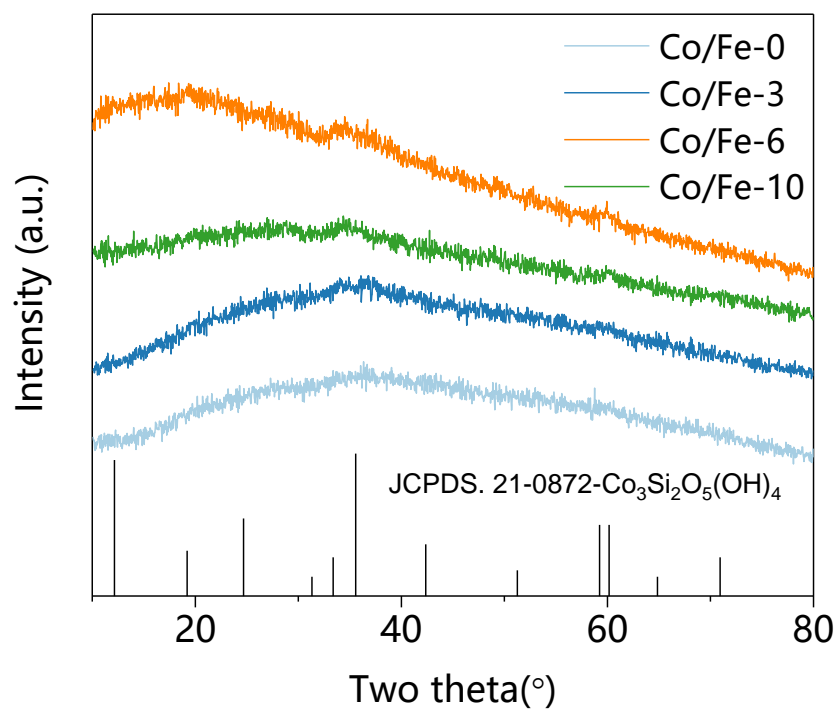


Figure S4. XRD patterns of CSHNs, FCSHNs-3, FCSHNs-6, and FCSHNs-10.

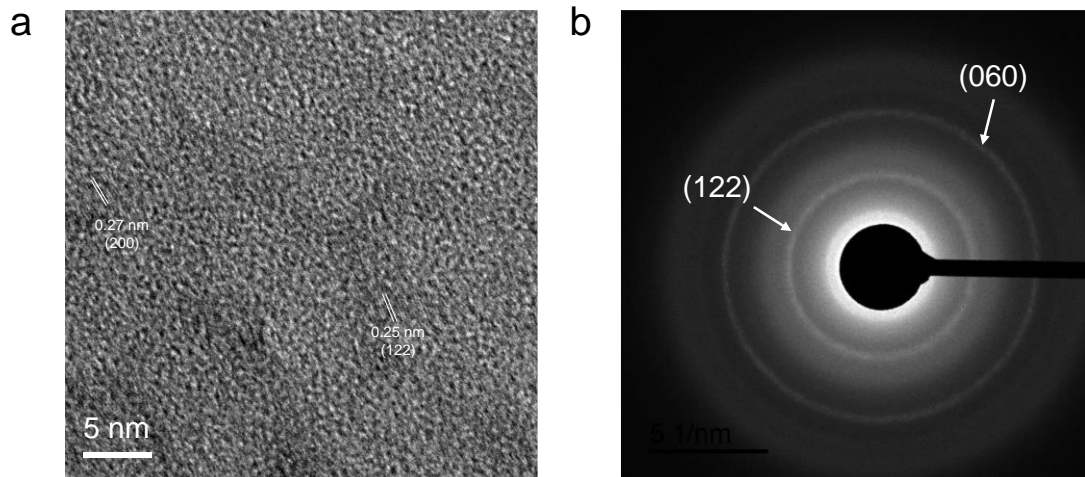


Figure S5. HRTEM image (a) and SAED pattern (b) of FCSHNs-6.

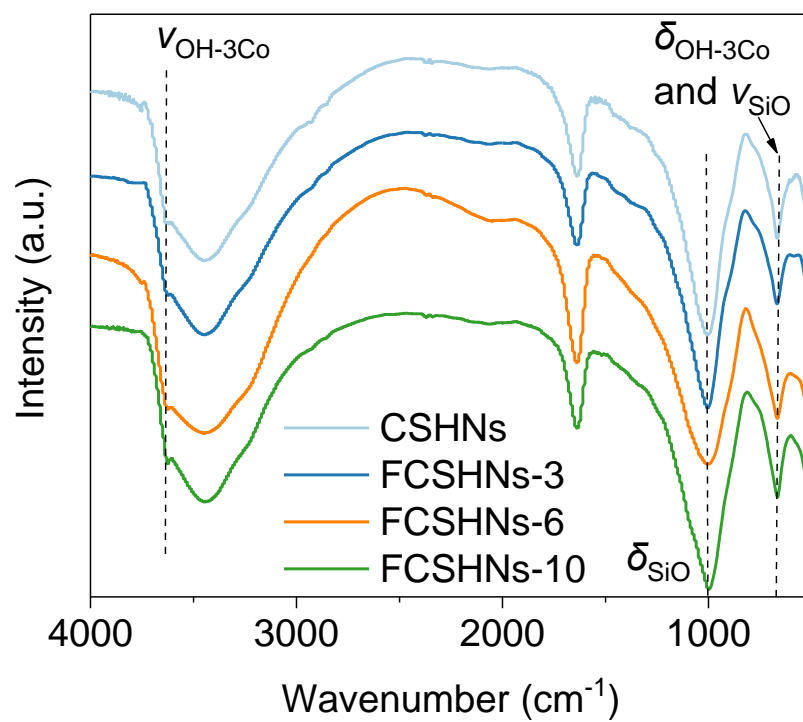


Figure S6. FT-IR spectra of CSHNs, FCSHNs-3, FCSHNs-6, and FCSHNs-10.

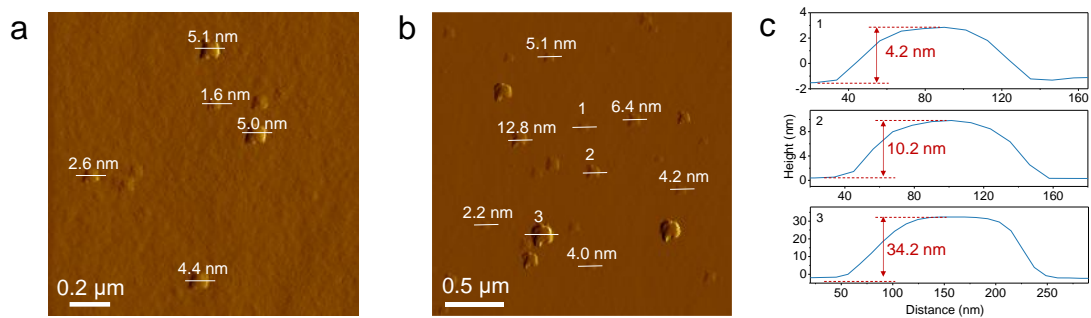


Figure S7. (a) AFM image of CSHNs; (b) AFM image of FCSHNs-6 and (c) the corresponding height profiles (the numbers from 1 to 3 in c correspond to the numbers from 1 to 3 in b).

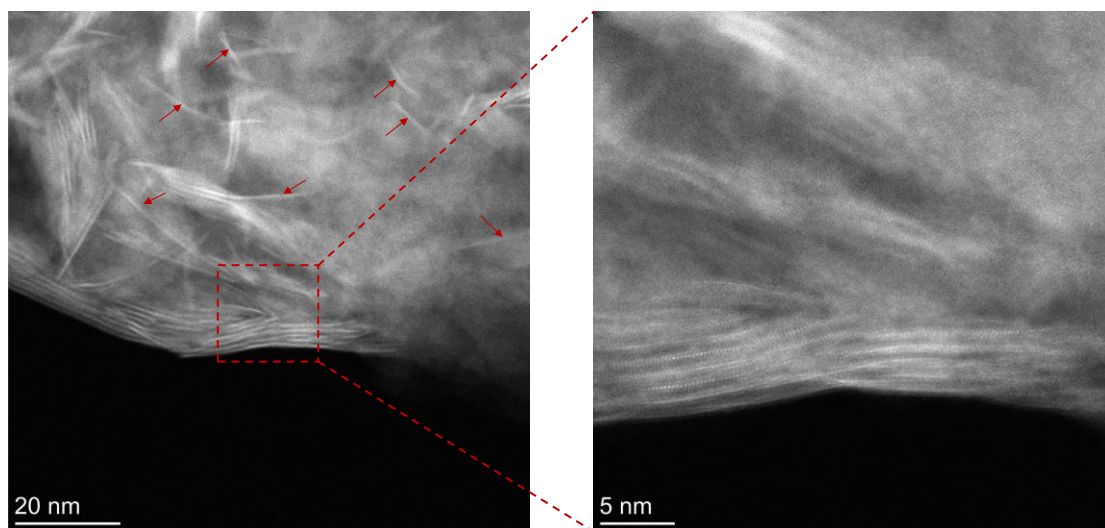


Figure S8. HADDF-STEM images of FCSHNs-6. The arrows indicate the single-layer nanosheets.

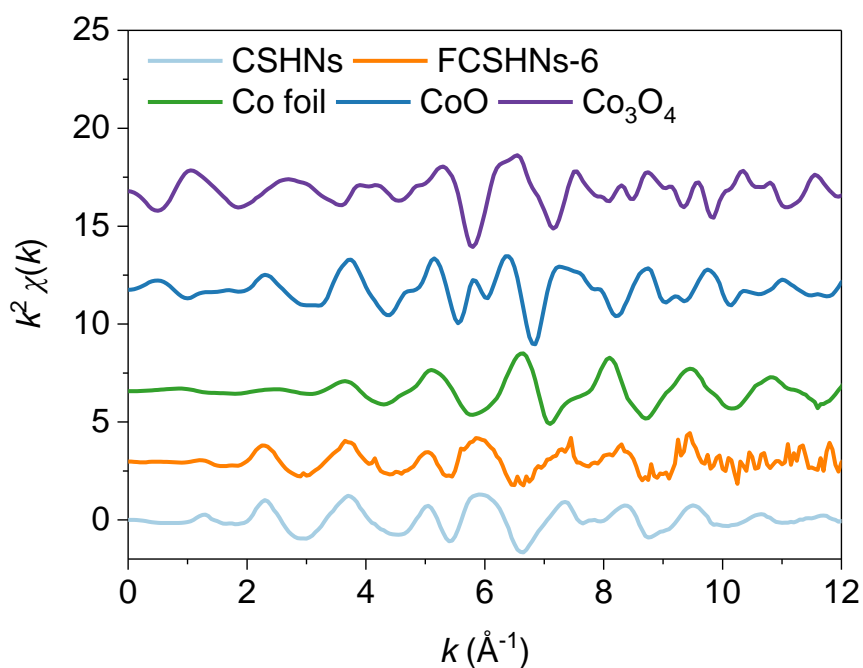


Figure S9. Co K-edge EXAFS oscillation functions $k^2\chi(k)$.

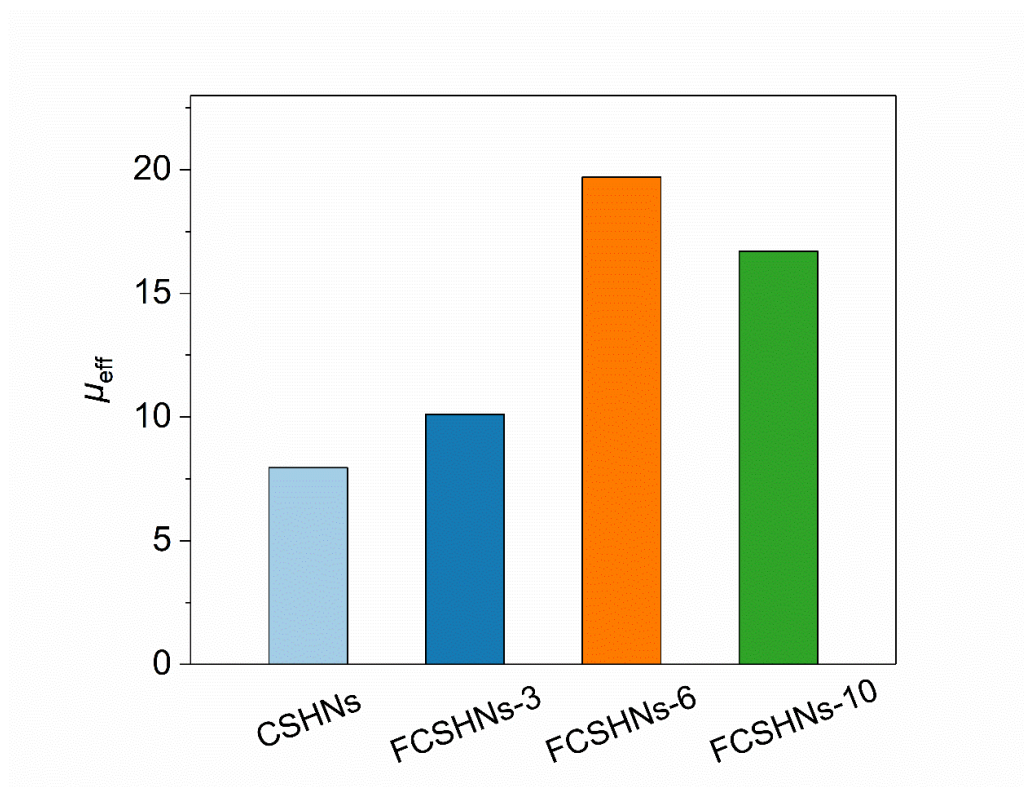


Figure S10. The calculated effective magnetic moment of CSHNs, FCSHNs-3, FCSHNs-6, and FCSHNs-10. The effective magnetic moment μ_{eff} was obtained by fitting the temperature dependence of susceptibilities and was calculated through the following equation: $\mu_{\text{eff}} = \sqrt{8C} \mu_{\text{B}}$.

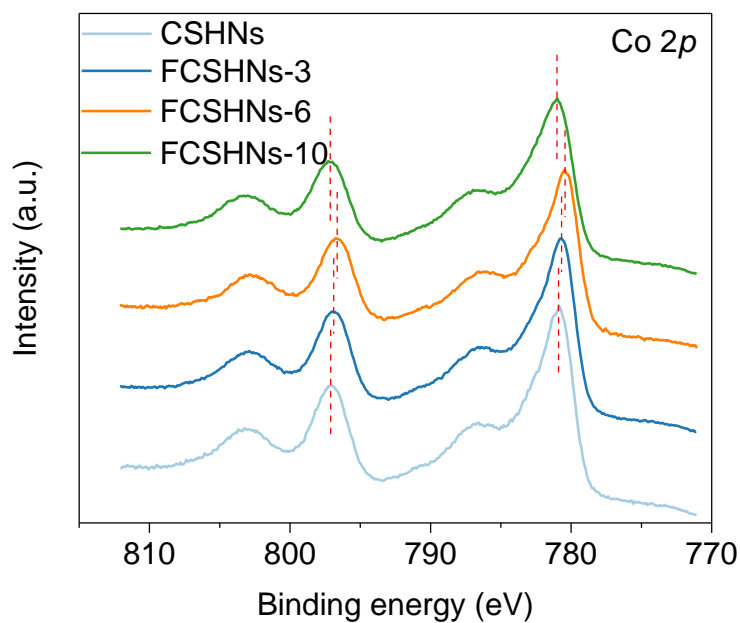


Figure S11. High-resolution Co 2p XPS spectra for CSHNs, FCSHNs-3, FCSHNs-6, and FCSHNs-10.

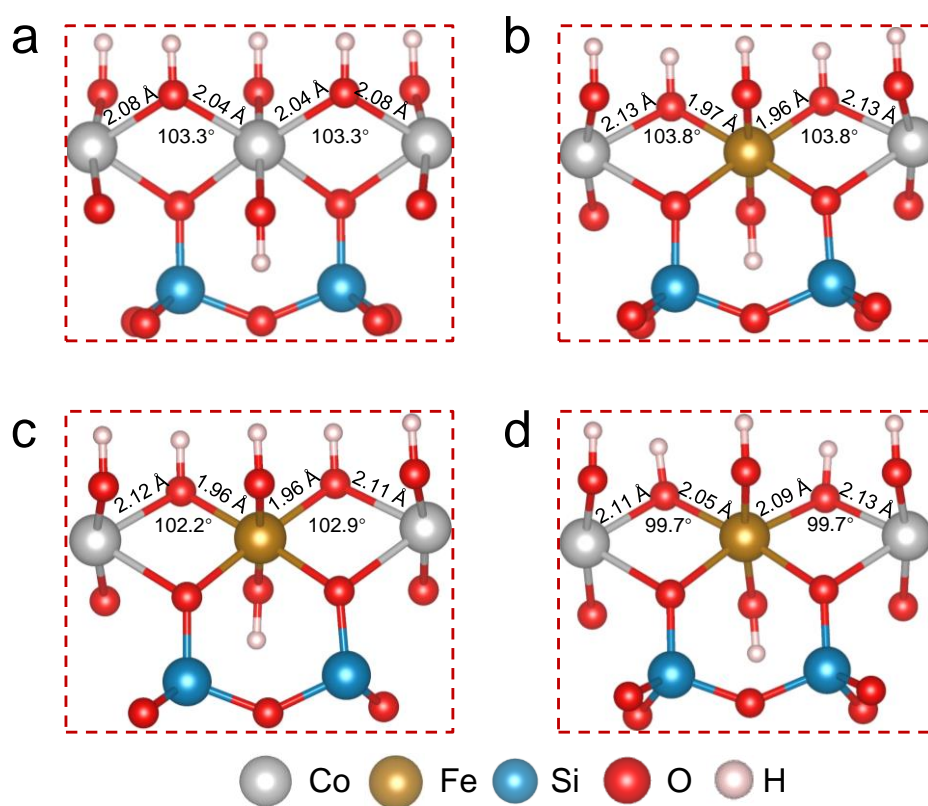


Figure S12. Structural models of (a) CSHNs, (b) FCSHNs-3, (c) FCSHNs-6 and (d) FCSHNs-10. The ball represents different elements. Silver: Co; Brown: Fe; Blue: Si; Red: Oxygen; Pink: H.

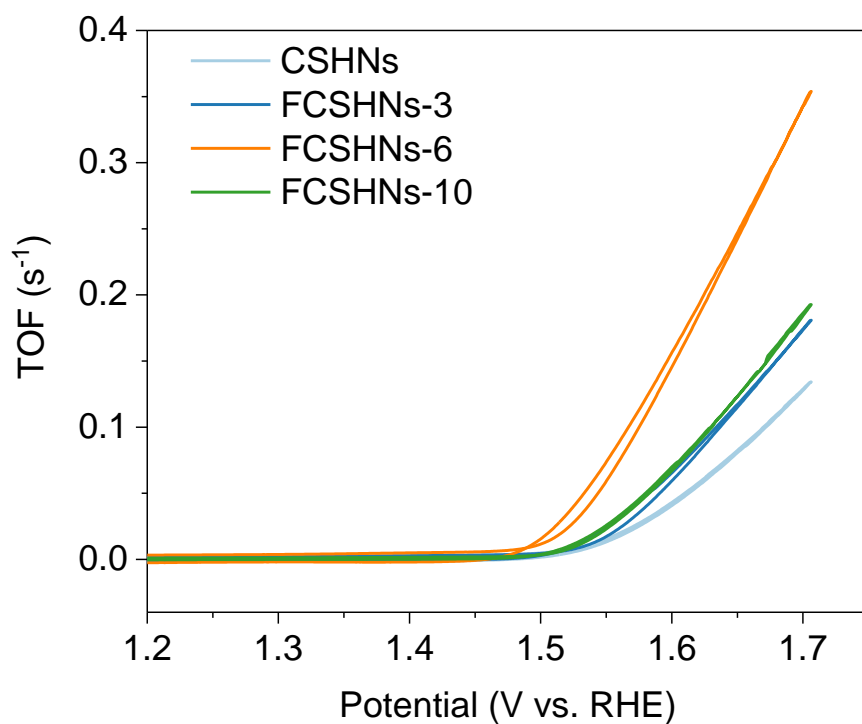


Figure S13. The turnover frequency of all samples.

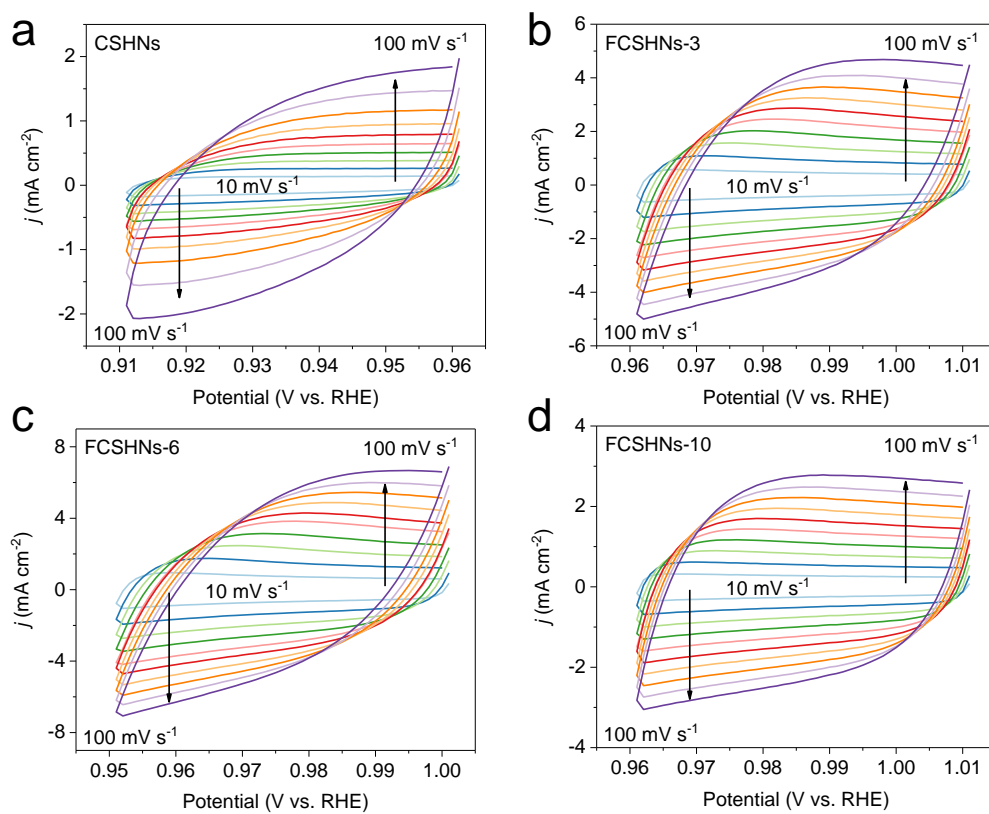


Figure S14. CV curves at different scan rates of (a) CSHNs, (b) FCSHNs-3, (c) FCSHNs-6, and (d) FCSHNs-10.

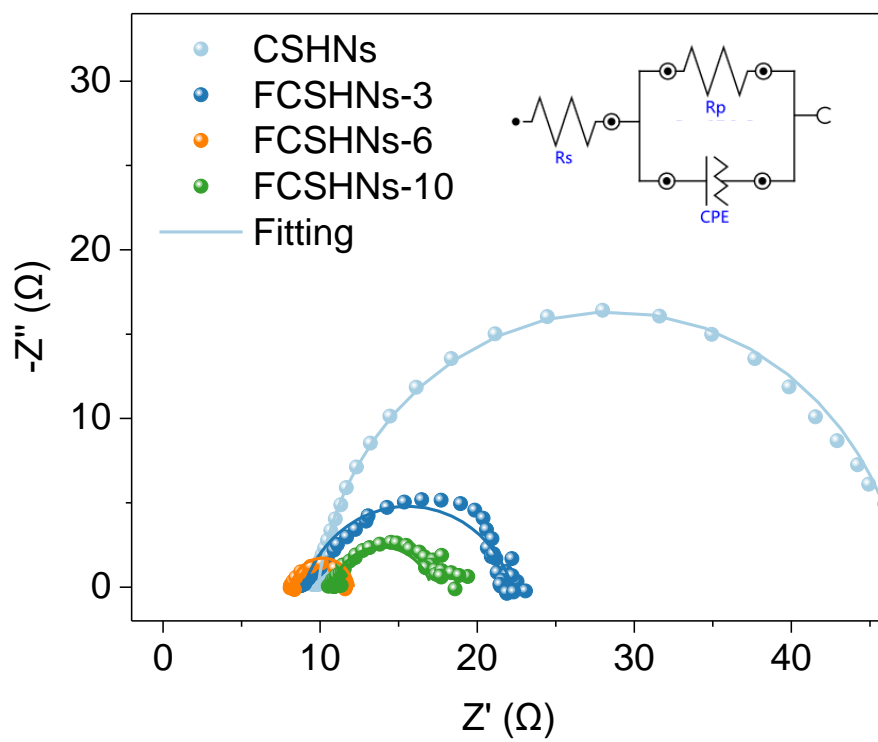


Figure S15. EIS curves of CSHNs, FCSHNS-3, FCSHNS-6, and FCSHNS-10 in O_2 -saturated 1.0 M KOH.

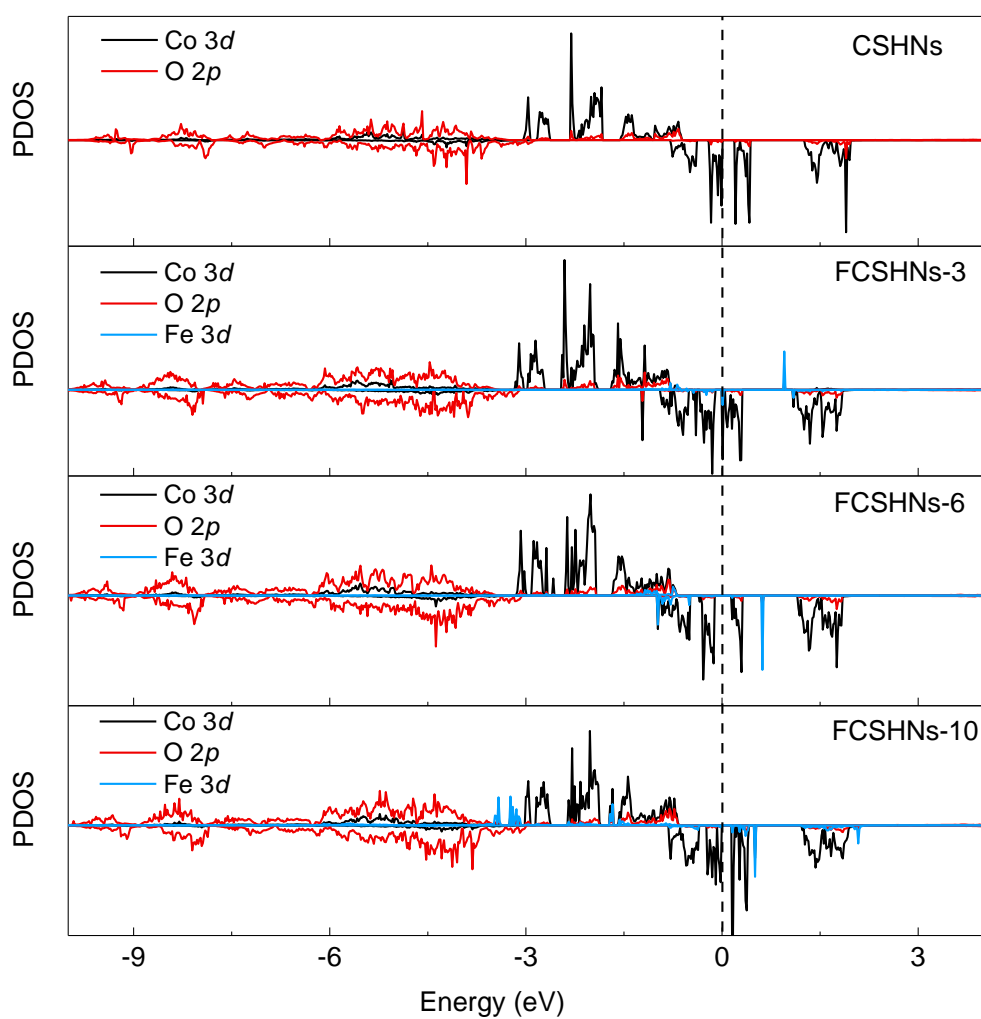


Figure S16. Calculated partial density of states (PDOS) reflecting the contributions of different atomic orbitals for CSHNs, FCSHNS-3, FCSHNS-6, and FCSHNS-10.

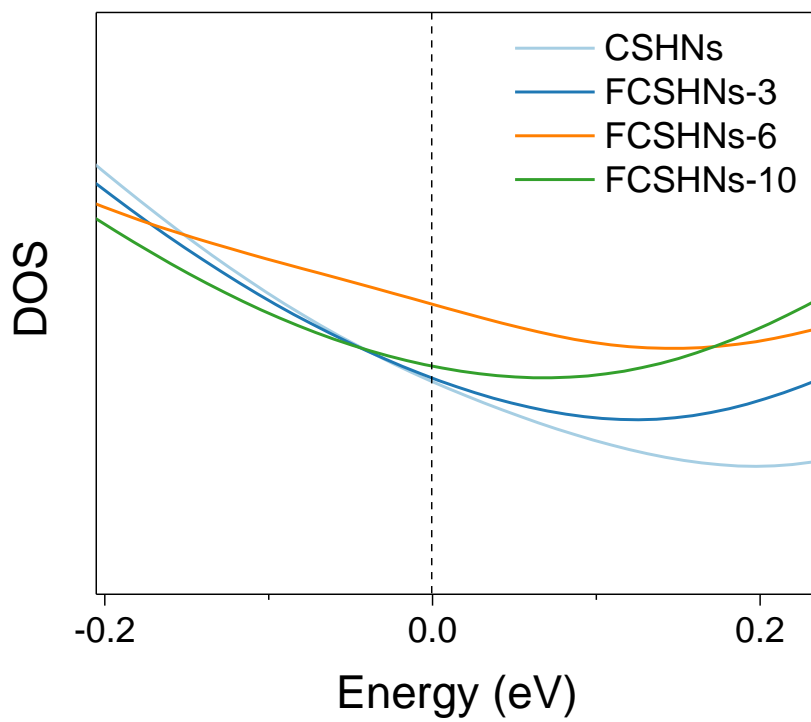


Figure S17. Calculated PDOS for Co 3*d* band.

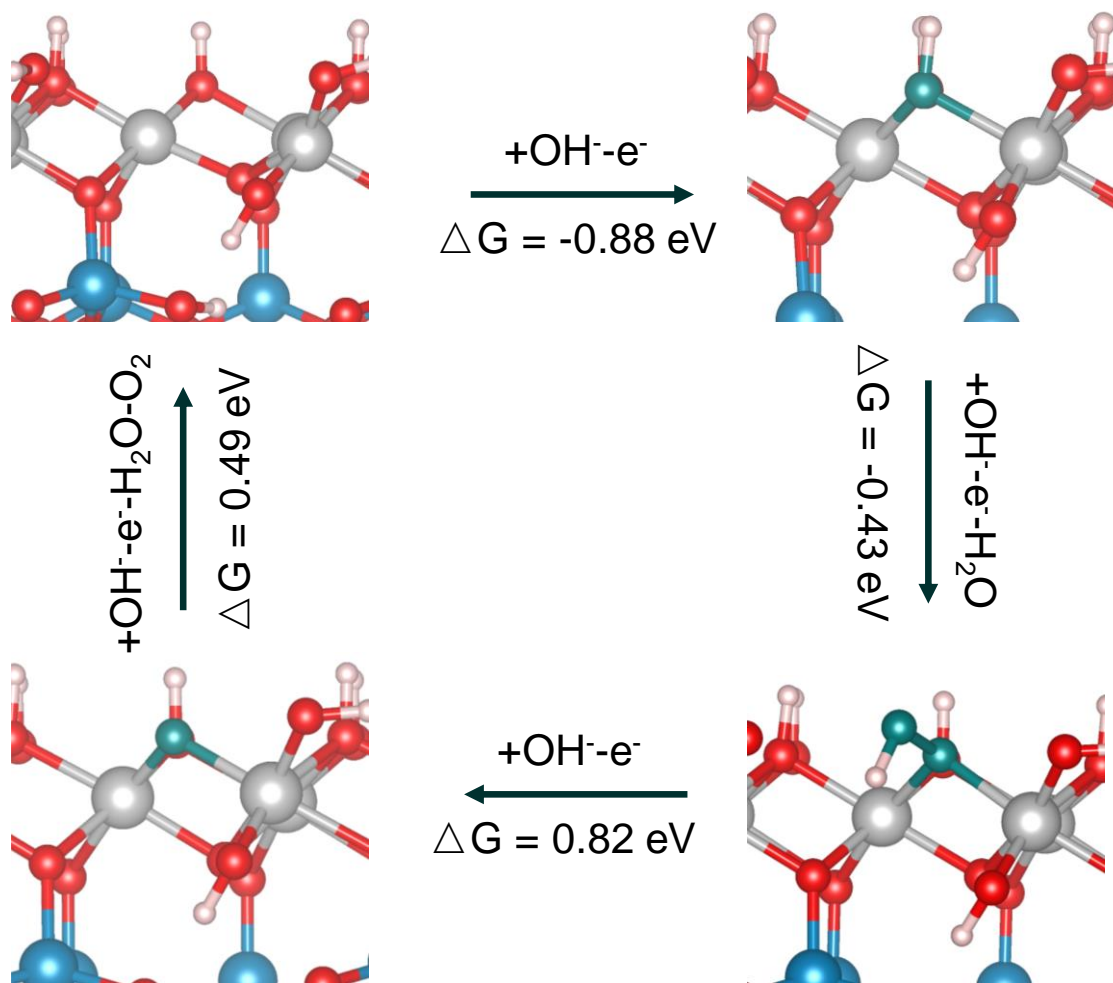


Figure S18. OER pathways and calculated free energy on the surface of CSHNs.

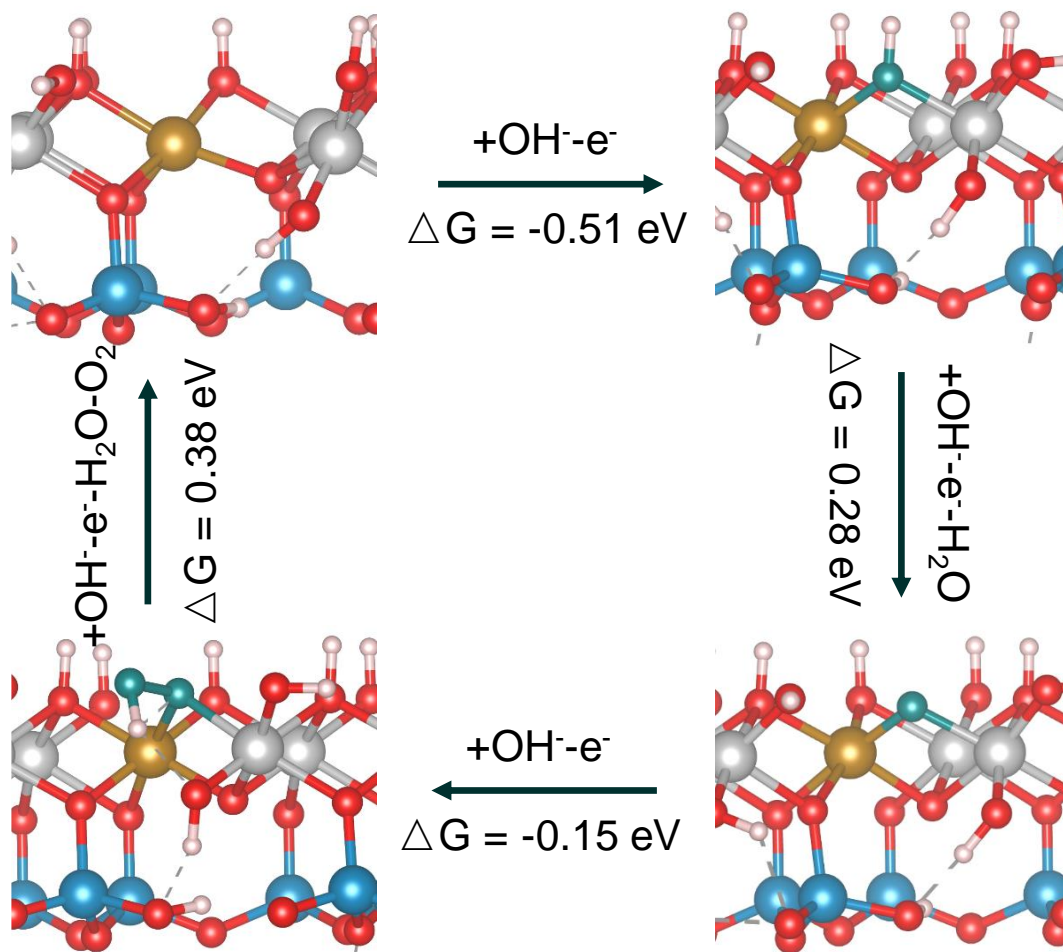


Figure S19. OER pathways and calculated free energy on the surface of FCSHNs-6.

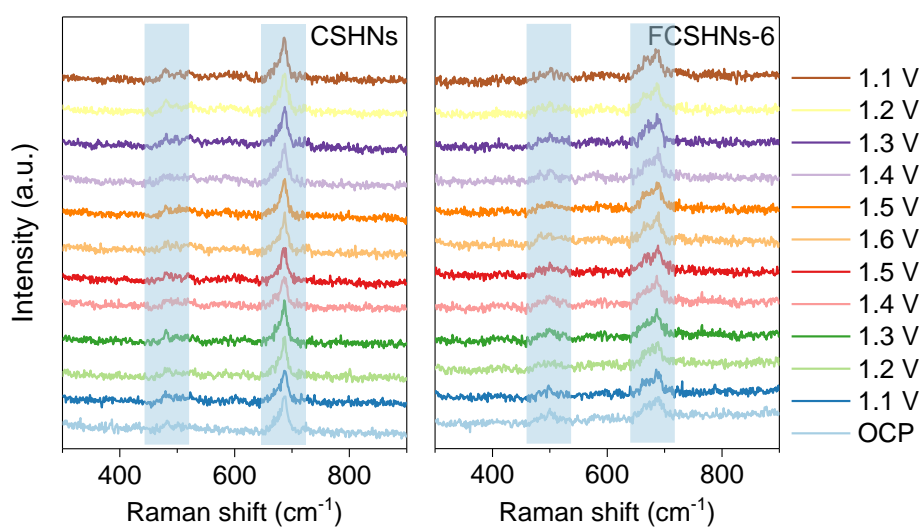


Figure S20. In situ Raman spectra of CSHNs and FCHNs-6 under OER condition.

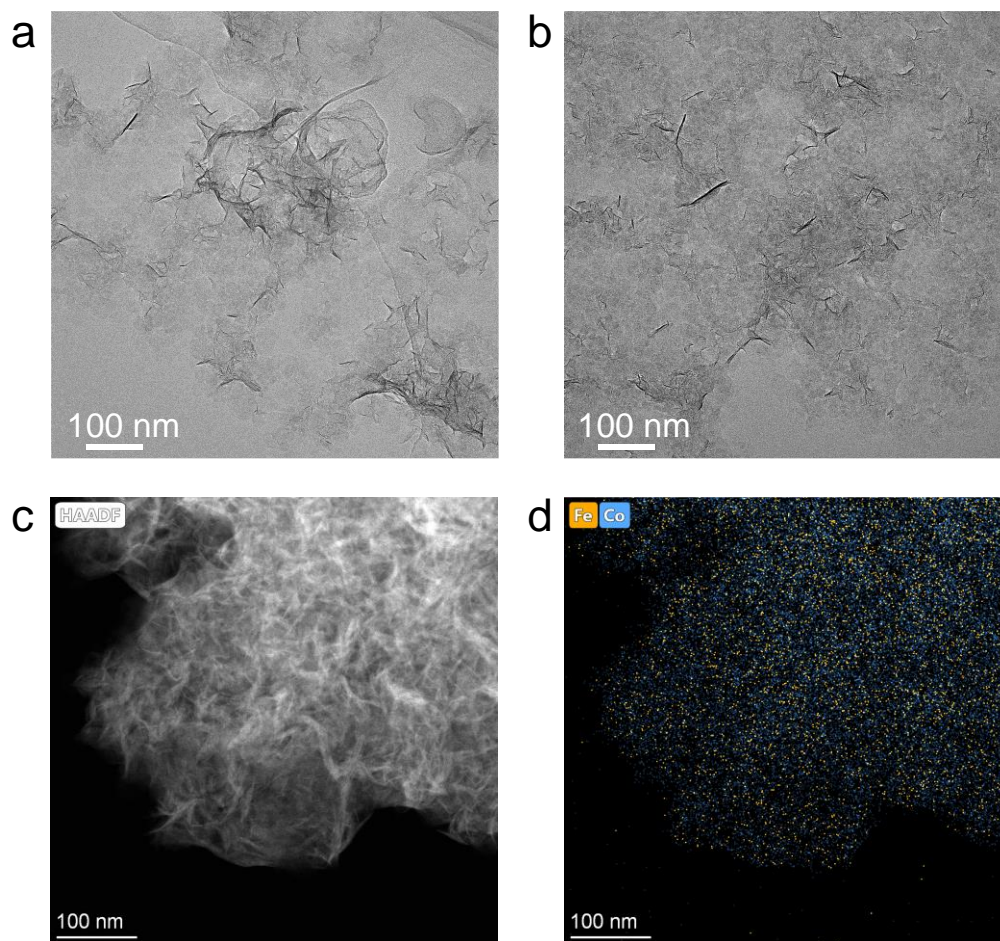


Figure S21. TEM images of (a) CSHNs and (b) FCSHNs-6 after OER test; (c-d) The HAADF-STEM image and corresponding EDS mapping of FCSHNs-6 after OER test.

Table S1. Comparison of OER performance of CSHNs and FCSHNs with bimetal oxide and hydroxide electrocatalysts recently reported.

| Catalysts | Electrolytes | Substrate | Overpotential at specific current density | Tafel slope (mV dec ⁻¹) | Reference |
|--|--------------|------------------|---|-------------------------------------|-----------|
| CSHNs | 1 M KOH | GCE ^a | 367 mV at 10 mA cm ⁻² | 75.1 | This work |
| FCSHNs-3 | 1 M KOH | GCE | 339 mV at 10 mA cm ⁻² | 66 | This work |
| FCSHNs-6 | 1 M KOH | GCE | 293 mV at 10 mA cm ⁻² | 47.2 | This work |
| FCSHNs-10 | 1 M KOH | GCE | 335 mV at 10 mA cm ⁻² | 66.2 | This work |
| Ultrathin Co–Mn LDH | 1 M KOH | GCE | 324 mV at 10 mA cm ⁻² | 43 | [14] |
| SNCF-BM | 0.1 M KOH | GCE | 420 mV at 10 mA cm ⁻² | 90 | [15] |
| Co–Fe LDH/rGO | 0.1 M KOH | GCE | 330 mV at 7.75 mA cm ⁻² | 43 | [16] |
| Co–Fe LDH (1:0.35) | 0.1 M KOH | GCE | 350 mV at 10 mA cm ⁻² | 49 | [18] |
| Co–Fe LDH (Plasma) | 1 M KOH | GCE | 290 mV at 10 mA cm ⁻² | 36 | [20] |
| CoFe ₂ O ₄ (V _O) | 1 M KOH | GCE | 280 mV at 1 mA cm ⁻² | 48 | [21] |
| SFNM-5% H ₂ /Ar | 0.1 M KOH | GCE | 359 mV at 10 mA cm ⁻² | 59 | [22] |
| Co ₂ FeO ₄ /NCNTs | 0.1 M KOH | GCE | 420 mV at 10 mA cm ⁻² | 96.7 | [23] |
| ACFP64 | 1 M KOH | GCE | 329 mV at 10 mA cm ⁻² | 35.9 | [24] |

^aGCE = glass carbon electrode.

Reference

- [1] P. E. Blöchl, O. Jepsen, O. K. Andersen, *Phys. Rev. B* **1994**, *49*, 16223.
- [2] G. Kresse, J. Furthmüller, *Comp. Mater. Sci.* **1996**, *6*, 15.
- [3] J. P. Perdew, W. Yue, *Phys. Rev. B* **1986**, *33*, 8800.
- [4] J. P. Perdew, K. Burke, M. Ernzerhof, *Phys. Rev. Lett.* **1996**, *77*, 3865.
- [5] P. E. Blöchl, *Phys. Rev. B* **1994**, *50*, 17953.
- [6] G. Kresse, D. Joubert, *Phys. Rev. B* **1999**, *59*, 1758.

- [7] H. J. Monkhorst, J. D. Pack, *Phys. Rev. B* **1976**, *13*, 5188.
- [8] M. Methfessel, A. T. Paxton, *Phys. Rev. B* **1989**, *40*, 3616.
- [9] J. B. Goodenough, R. Manoharan, M. Paranthaman, *J. Am. Chem. Soc.* **1990**, *112*, 2076.
- [10] J. S. Kim, I. Park, E.-S. Jeong, K. Jin, W. M. Seong, G. Yoon, H. Kim, B. Kim, K. T. Nam, K. Kang, *Adv. Mater.* **2017**, *29*, 1606893.
- [11] E. P. L. Hunter, S. G. Lias, *J. Phys. Chem. Ref. Data* **1998**, *27*, 413.
- [12] J. K. Nørskov, J. Rossmeisl, A. Logadottir, L. Lindqvist, J. R. Kitchin, T. Bligaard, H. Jónsson, *J. Phys. Chem. B* **2004**, *108*, 17886.
- [13] Z. Lu, W. Xu, W. Zhu, Q. Yang, X. Lei, J. Liu, Y. Li, X. Sun, X. Duan, *Chem. Commun.* **2014**, *50*, 6479.
- [14] F. Song, X. Hu, *J. Am. Chem. Soc.* **2014**, *136*, 16481.
- [15] Y. Zhu, W. Zhou, Z. G. Chen, Y. Chen, C. Su, M. O. Tadé, Z. Shao, *Angew. Chem. Int. Ed.* **2015**, *54*, 3897.
- [16] X. Han, C. Yu, J. Yang, C. Zhao, H. Huang, Z. Liu, P. M. Ajayan, J. Qiu, *Adv. Mater. Inter.* **2016**, *3*, 1500782.
- [17] D. Guo, J. Qi, W. Zhang, R. Cao, *ChemSusChem* **2017**, *10*, 394.
- [18] F. Yang, K. Sliozberg, I. Sinev, H. Antoni, A. Bähr, K. Ollegott, W. Xia, J. Masa, W. Grünert, B. R. Cuenya, *ChemSusChem* **2017**, *10*, 156.
- [19] S. Zhao, Y. Wang, J. Dong, C.-T. He, H. Yin, P. An, K. Zhao, X. Zhang, C. Gao, L. Zhang, J. Lv, J. Wang, J. Zhang, A. M. Khattak, N. A. Khan, Z. Wei, J. Zhang, S. Liu, H. Zhao, Z. Tang, *Nat. Energy* **2016**, *1*, 16184.
- [20] R. Liu, Y. Wang, D. Liu, Y. Zou, S. Wang, *Adv. Mater.* **2017**, *29*, 1701546.
- [21] K.-L. Yan, X. Shang, Z.-Z. Liu, B. Dong, S.-S. Lu, J.-Q. Chi, W.-K. Gao, Y.-M. Chai, C.-G. Liu, *Int. J. Hydrogen Energ.* **2017**, *42*, 24150.
- [22] K. Zhu, T. Wu, M. Li, R. Lu, X. Zhu, W. Yang, *J. Mater. Chem. A* **2017**, *5*, 19836.
- [23] X. T. Wang, T. Ouyang, L. Wang, J. H. Zhong, T. Ma, Z. Q. Liu, *Angew. Chem. Int. Ed.* **2019**, *131*, 13425.
- [24] B. Kim, J. S. Kim, H. Kim, I. Park, W. M. Seong, K. Kang, *J. Mater. Chem. A* **2019**, *7*, 18380.